DREAM: A Toolbox to Decode Rhythms of the Brain System

Zhu-Qing Gong[1,2,#], Peng Gao[3,#], Xiu-Xia Xing[4], Chao Jiang[2,5], Tonya White[6,7], F. Xavier Castellanos[8,9], Hai-Fang Li[3,*], Xi-Nian Zuo[1,2,5,10,11,12*]

1. Department of Psychology, University of Chinese Academy of Sciences (UCAS), Beijing, China
2. Key Laboratory of Behavioral Sciences, CAS Institute of Psychology, Beijing, China
3. School of Computer Sciences, Taiyuan University of Technology, Taiyuan, China
4. College of Applied Sciences, Beijing University of Technology, Beijing, China
5. Research Center for Lifespan Development of Brain and Mind (CLIMB), CAS Institute of Psychology, Beijing, China
6. Department of Child and Adolescent Psychiatry, Erasmus University, Rotterdam, Netherlands
7. Department of Radiology, Erasmus University Medical Centre, Rotterdam, Netherlands
8. Langone Medical Center, Child Study Center, New York University, New York, USA
9. Nathan S. Kline Institute for Psychiatric Research, Orangeburg, New York, USA
10. Magnetic Resonance Imaging Research Center, CAS Institute of Psychology, Beijing, China
11. Key Laboratory for Brain and Education Science, Nanning Normal University, Nanning, China
12. IDG/McGovern Institute for Brain Research & National Laboratory of Cognitive Sciences and Learning, Beijing Normal University, Beijing, China

#Contribute equally as the first author

***Corresponding authors:**

Xi-Nian Zuo, PhD,

Center for Developmental Population Neuroscience

Beijing Normal University

Research Center for Lifespan Development of Brain and Mind

University of Chinese Academy of Sciences

Emails: zuoxinian@gmail.com; zuoxn@psych.ac.cn
Office/Fax: +86 10 64853798; Cell: +86 13810191181

Hai-Fang Li, PhD, Taiyuan University of Technology
Email: lihaifeng@tyut.edu.cn
Cell: +86 15340682795

Abstract

Rhythms of the brain are generated by neural oscillations across multiple frequencies. Following the natural log linear law of frequency distribution, these oscillations can be decomposed into distinct frequency intervals associated with specific physiological processes. This perspective on neural oscillations has been increasingly applied to study human brain function and related behaviors. In practice, relevant signals are commonly measured as a discrete time series, and thus the sampling period and number of samples determine the number and ranges of decodable frequency intervals. However, these limits have been often ignored by researchers who instead decode measured oscillations into multiple frequency intervals using a fixed sample period and numbers of samples. One reason for such misuse is the lack of an easy-to-use toolbox to implement automatic decomposition of frequency intervals. We report on a toolbox with a graphical user interface for achieving local and remote decoding rhythms of the brain system (DREAM) which is accessible to the public via GITHUB. We provide worked examples of DREAM used to investigate frequency-specific performance of both neural (spontaneous brain activity) and neurobehavioral (in-scanner head motion) oscillations. Using the imaging data from the Human Connectome Project, DREAM mapped the amplitude of these neural oscillations into multiple frequency bands as well as their test-retest reliability. DREAM analyzed the head motion oscillation and found that younger children moved their heads more than older ones across all five frequency intervals, particularly in the higher frequency intervals. In the age interval from 7 to 9 years, boys moved more than girls across all frequency intervals. Such sex-related motion effects were not detectable for other ages. These findings demonstrate the applicability of DREAM for frequency-specific human brain mapping.

Keywords: neural oscillations, frequency intervals, reliability, amplitude, head motion

1 Introduction

Rhythms of the brain are generated by neural oscillations occurring across multiple frequencies. The natural logarithm linear law (N3L) offers a template for parcellating these neural oscillations into multiple frequency intervals linked with distinct physiological roles (Penttonen & Buzsáki, 2003). Remarkably, when graphed on the natural logarithm scale, the centers of each frequency interval fall on adjacent integer points. Thus, distances between adjacent center points are isometric on the natural logarithm scale, resulting in a full parcellation of the whole frequency domain where each parcel of the frequencies is fixed in theory, namely frequency intervals. These frequency intervals have been repeatedly observed experimentally (Buzsaki & Draguhn, 2004). This characteristic suggests that distinct physiological mechanisms may contribute to distinct intervals. Functional magnetic resonance imaging (fMRI), a non-invasive and safe technique with an acceptable tradeoff between spatial and temporal resolution, has the potential to contribute to the study of certain neural oscillations in the human brain in vivo. In early fMRI studies of the human brain, researchers tended to treat oscillations across different frequencies without differentiation. Low-frequency oscillations measured by resting-state fMRI (rfMRI) have been assessed primarily in the frequency range of 0.01 to 0.1 Hz, a range in which spontaneous brain activity has high signal amplitude (Biswal et al., 1995; Lowe et al., 1998). While such efforts have been somewhat informative, treating this broad frequency range in a unitary manner may conceal information carried by different frequency intervals. To address this issue,

an early study decomposed the rfMRI signals into multiple frequency intervals using the N3L theory (slow-5: 0.01 - 0.027 Hz, slow-4: 0.027 - 0.073 Hz, slow-3: 0.073 - 0.198 Hz, slow-2: 0.198 - 0.25 Hz) (Zuo et al., 2010). This exploration demonstrated the feasibility of mapping distributional characteristics of oscillations' amplitude in both space and time across multiple frequency intervals in the brain.

Since then, an increasing number of rfMRI studies have employed such methods by directly applying these frequency intervals, and have detected frequency-dependent differences in brain oscillations in patients. Specifically, these differences were mostly evident between slow-4 and slow-5 amplitudes (Han et al., 2011; Jing et al., 2012; Zhao et al., 2015; Mascali et al., 2015; Ren et al., 2016; Li et al., 2017). Such frequency-dependent phenomena have also been explored using other rfMRI metrics including regional homogeneity (Wang et al., 2016) detected in the slow-3 and slow-5 frequency ranges. While the lower and upper bounds of the frequency intervals are fixed in theory, their highest and lowest detectable frequencies and frequency resolution are determined by the sampling parameters (e.g., rate and duration) in computational practice. However, the above-mentioned studies applied the frequency intervals from earlier studies (Di Martino et al., 2008; Zuo et al., 2010) rather than to use those matching their actual sampling settings. To address this situation, we developed an easy to use toolbox to decode the frequency intervals by applying the N3L theory. This toolbox, named DREAM, is based on MATLAB with a graphical user interface (GUI). Here, we introduce the N3L algorithm and its DREAM implementation. Neural oscillations reflected by the human brain spontaneous activity measured with resting-state functional MRI and head motion data during mock MRI scans were employed as two worked examples to demonstrate the use of DREAM to perform frequency analyses.

2 Methods and Algorithms

Neuronal brain signals are temporally continuous but they are almost always measured as discrete data for practical reasons. The characteristics of the sampled data should meet the criterion of the sampling theorem proposed by American electrical engineers Harry Nyquist and Claude Shannon. The core algorithm to determine the frequency boundaries of measured neuronal signals in DREAM is based on the Nyquist-Shannon sampling theorem. Specifically, per the theorem, sampling frequency and sampling time determine the highest and lowest frequencies that can be detected and reconstructed. Sampling data retains most of the information contained in the original signals if the sampling frequency is at least twice the maximum frequency of the continuous signals. As for neuronal signals, the highest frequency that could be detected and reconstructed is determined by the sampling frequency, or by the sampling interval which is equal to the reciprocal of the sampling frequency, as shown in formula (1):

$$f_{max} = \frac{1}{2T_R} \quad (1)$$

where f_{max} represents the highest frequency that could be detected in the neuronal signal and T_R represents the sampling interval.

The lowest frequency in neuronal signals that could be detected depends on the sampling time. As shown in formula (2), in order to distinguish the lowest frequency in

neuronal signals, the sampling time should be equal to or larger than the reciprocal of two times the lowest frequency:

$$T \geq \frac{1}{2f_{min}} \quad (2)$$

where T represents the sampling time, and f_{min} represents the lowest frequency in neuronal signals that could be distinguished.

Since the sampling time is equal to the number of samples multiplied by the sampling interval, the lowest frequency can be calculated by formula (3):

$$f_{min} = \frac{1}{2NT_R} \quad (3)$$

where *N* represents the number of samples.

According to the N3L theory, neural oscillations in mammalian brain formed a linear hierarchical organization of multiple frequency bands when regressed on a natural logarithmic scale. The center of each band would fall on each integer of the natural logarithmic scale (Fig. 1-1). Thus, adjacent bands have constant intervals that equals to one, which correspond to the approximately constant ratios of adjacent bands on the linear scale (Fig. 1-2). With the highest and lowest frequencies reconstructed, N3L can derive the number of decoded frequencies and the boundaries of each frequency interval (Fig. 1-3). Accordingly, when graphed on the natural log scale, the center of each decoded frequency is an integer. Thus, adjacent center points on the natural log scale are equidistant, which corresponds to the same proportion of adjacent center points' values on the linear scale. Based upon this theorem, after performing a linear regression analysis for the highest and lowest frequencies acquired previously, we can determine the central frequencies, as well as the number frequency intervals that can be decoded.

Finally, the decoding process integrated in DREAM performs band-pass filtering with the frequency intervals provided by DREAM in the previous steps (Fig. 1-4). This is implemented by the MATLAB built-in function *fft* and *ifft* to perform direct and inverse time-frequency transformation on the signals for individual decoded frequency intervals, respectively. All the above steps are illustrated as the flowchart in Figure 1.

3 DREAM Interface and Usage

3.1 Program Interface

DREAM is currently being shared at GITHUB[1] as part of the Connectome Computation System (Xu et al., 2015). After downloading the package, users will need to add the directory where the package is stored into the MATLAB path. The package can then be launched by entering "DREAM" in the MATLAB command line. DREAM has a GUI on its welcome screen (Fig. 2) and main interface (Fig. 3). On the left side of the main interface, users can set up the required parameters. On the right side, a large view frame previews the plots of time series from the data selected. Data should be entered in the structure shown in Figure 4 before processing. The *work directory* is where the

[1]https://github.com/zuoxinian/CCS/tree/master/H3/DREAM

subject directories are stored (full path). Data should be stored in each *subject directory* or a sub-folder inside (*data directory*).

3.2 GUI Usage

We introduce how to use the graphical interface step by step. The circled numbers in Figure 3 correspond to the analyzing steps in this section.

1) Step 1 - *select the data type*: Click the drop-down box to choose the data type to be analyzed.
2) Step 2 - *set up the work directory*: Click the path selection button to set the work directory in the dialog box that pops up.
3) Step 3 - *batch process*: Select the subject list file in the popped-up dialog box by clicking the file selection button.
4) Step 4 - *set up sampling rate*: Enter the sampling interval in seconds (T_R) in the input box (in some cases, this can be automatically extracted from the header information).
5) Step 5 (optional) - *data directory*: If the data are stored in a sub-folder inside the subject directory, type the name of the data directory in the input box.

After all the above parameters are set up, data meeting the requirement will appear in the list-box (Fig. 3-6), from where the user can remove unwanted data by selecting the file name and clicking the *Remove* button. Finally, by clicking the *Divide* button, a user can start the decoding program. The outputs contain a set of decoded files and a csv file that records the boundary frequencies of each decoded band. The outcomes can be directly used for subsequent analyses. To demonstrate the DREAM use, we employed it for a multi-band frequency analysis assessing head motion during mock scanning.

4 DREAM Demo1: Head motion in youth during mock scanning

In-scanner head motion has been treated as a confound in fMRI studies, especially in studies of children and patients with psychiatric disorders. Many studies have shown the effects of motion on fMRI results such as increases of short-distance correlations and decreases of long-distance correlations in rfMRI (Power et al., 2012; Yan et al., 2013). Researchers have proposed various methods to correct motion effects in fMRI studies. In contrast, studying head motion as a neurobehavioral trait has long been overlooked (see an exception in Zeng et al., 2014), especially in children. Here, we use DREAM to quantify head motion data acquired from children in a mock scanner using a novel multi-frequency perspective. We hypothesized that: 1) head motion is a trait associated with age; 2) there are sex differences in head motion in children; and 3) there may be frequency-dependent motion effects.

4.1 Participants and data acquisition

We recruited 94 participants (47 females) between 3 to 16 years of age as part of the Chinese Color Nest Project (Yang et a., 2017; Zuo et al., 2017), a long-term (2013-2022) large-scale program[2] from the Research Center for Lifespan Development of Mind and Brain (CLIMB)[3]. All participants were from groups visiting during the

[2]http://zuolab.psych.ac.cn/colornest.html
[3]https://climbgroup.org

Science Open Day of the Chinese Academy of Sciences, with the approval of at least one legal guardian. The experiment was performed in a mock MRI scanner at the site of the MRI Research Center of the CAS Institute of Psychology (Fig. 5). The mock scanner was built by PST (Psychology Software Tools, Inc.) using a 1:1 model of the GE MR750 3T MRI scanner in use at the institute. It is used for training young children to lie still in a scanner before participating the actual MRI scanning session. It is decorated with cartoon stickers to provide a children-friendly atmosphere. Head motion data were acquired with the MoTrack Head Motion Tracking System (PST-100722). The system consists of three components: a MoTrack console, a transmitter and a sensor. The sensor is worn on the participant's head and provides the position of the head relative to the transmitter. For each participant, head motion is displayed on the computer screen in real-time. The original sampling rate of the system is 103 Hz. The averaging buffering size is 11 samples, which results in a recording sampling rate of 9.285 Hz. The participants were instructed to rest quietly on the bed of the mock scanner for around three and half minutes without moving their heads or bodies. They were watching a cartoon film inside the scanner during the "scanning" to simulate movie-watching scanning. The data acquisition period was designed to resemble the real MRI scanning environment, with a recording of scanning noises of the real MRI machine played as the background noise.

4.2 Data analysis

Head motion data are recorded in text files consisting of six parameters for each time point, three translation (millimeters) and three rotation (degrees) measures. The first three parameters are displacements in the superior, left and posterior directions, respectively. The last three parameters are rotation degrees in the three cardinal rotational directions. We converted the original data into frame-wise displacement (FD), a single parameter scalar quantity representing head motion proposed by Power et al. (2012). To correct for spikes caused by sudden movements (data without this preprocessing was also analyzed), which may bias mean FD values, we applied the AFNI *3dDespike* command (version: AFNI_17.3.06, https://afni.nimh.nih.gov) to the FD time series. Then time-windows were determined and applied before feeding the data into DREAM. We retained 1672 sampling points from the zeroed time point (time point when the original six parameters were set to zero), which equaled a duration of three minutes. After preprocessing, we used DREAM to decode the data. Of note, the original FD values were all positive. After decoding, the time series of decoded bands were demeaned, which means the average values of all decoded time series were very near to zero. Thus, we took the absolute value of decoded frequency intervals to calculate mean FD values, which were used in subsequent statistical analyses. To assess the relationship between mean FD values and age, we fit data in each frequency interval with age and sex as covariates of interest, into the multivariable linear regression model in formula (4):

$$y = \beta_0 + \beta_1 x_1 + \beta_2 x_2 + \beta_3 x_1 x_2 \quad (4)$$

where y, x_1 and x_2 represent mean FD values, age and sex (as covariates) respectively, and β_0, β_1, β_2 and β_3 are regression coefficients. Of note, the age-sex interaction is modeled into the above equation as $x_1 x_2$. An analysis of variance (ANOVA) model with repeated measures and age and sex as variables of interests was also implemented.

We performed the Pearson's correlational analysis between the standard deviation of FD time series and age for each frequency band to see if the stability of head motion varies with age. To detect sex differences, we compared mean FD values of each decoded frequency intervals between males and females using two-sample t-tests.

4.3 Results

Six participants were excluded from further data analysis due to sampling periods under three minutes. Another four participants were excluded because their mean FD values were three standard deviations higher than the mean value of the whole group (outliers). In the end, 84 participants (42 females) were included in analyses. The demographic information of the final included participants is listed in Table 1. No significant differences in age were found between males and females. All the findings derived with the head motion data without *despike* preprocessing are highly similar to those of using *despike*, which are reported as following. Meanwhile, all the results derived from the multiple regression model are replicated by the ANOVA model.

Table 1 Demographic information of participants involved in analysis

Number	Sex	Mean Age	STD
42	Female	8.4	3.1
42	Male	8.7	3.0

4.3.1 Frequency decomposition

Since all the head motion data have the same sampling frequency and sampling period, DREAM decoded all the FD time series into the same five frequency intervals (F1: 0.033 to 0.083 Hz, F2: 0.083 to 0.22 Hz, F3: 0.222 to 0.605 Hz, F4: 0.605 to 1.650 Hz, F5: 1.650 to 4.482 Hz). Plots of the full band and the decoded frequency intervals from a participant are shown as an example in Figure 6 and Figure 7, respectively.

4.3.2 Relationship between age and head motion measures across frequencies

Results from linear regression analysis yielded significant negative correlations between age and mean FD values across all five bands (dof = 80, $p < 0.05$, FDR corrected p values: F1 0.025, F2 0.025, F3 0.022, F4 0.022, F5 0.018; adjusted R^2: F1 0.122, F2 0.159, F3 0.209, F4 0.202, F5 0.255). The relationship between age and mean FD values are plotted in Figure 8a. No sex effects were detectable for these correlations. This means younger children tend to move more than older ones, and this trait correlation held in both sexes. More details about predicted model coefficients are provided in Table 2, which provides raw p values without correction for multiple comparisons. In addition, we also performed a correlational analysis between the standard deviations of decoded FD values and age, and found similarly that the standard deviations were significantly negatively correlated with age (dof = 82, F1: $r = -0.319$, $p = 0.003$, $R^2 = 0.102$; F2: $r = -0.337$, $p = 0.002$, $R^2 = 0.114$; F3: $r = -0.417$, $p < 0.001$, $R^2 = 0.174$; F4: $r = -0.446$, $p < 0.001$, $R^2 = 0.199$; F5: $r = -0.488$, $p < 0.001$, $R^2 = 0.238$). This could indicate that there is less head motion variability with age.

Table 2 Regression models of mean FD values for the five frequency bands

		Estimate	T value	P
F1	β_0	0.089616	3.859	0.00023
	β_1	-0.006019	-2.305	0.02377*
	β_2	0.027346	0.806	0.42248
	β_3	-0.000647	-0.172	0.86377
F2	β_0	0.093527	4.073	0.000108
	β_1	-0.005900	-2.285	0.024949*
	β_2	0.044632	1.331	0.186960
	β_3	-0.002474	-0.666	0.507531
F3	β_0	0.080541	5.106	2.18e-06
	β_1	-0.004486	-2.529	0.0134*
	β_2	0.038527	1.673	0.0983
	β_3	-0.002686	-1.052	0.2958
F4	β_0	0.076823	6.192	2.41e-08
	β_1	-0.003564	-2.555	0.0125*
	β_2	0.027984	1.545	0.1264
	β_3	-0.002126	-1.059	0.2929
F5	β_0	0.088324	8.623	4.85e-13
	β_1	-0.003450	-2.995	0.00365*
	β_2	0.025042	1.674	0.09803
	β_3	-0.001922	-1.160	0.24966

4.3.3 Sex differences by age range

We first compared the mean FD values of each frequency interval between males and females. Females showed lower mean FD values than males across all the frequency intervals although the differences were not statistically significant. We divided participants into three age groups (3 to 6 years old, 7 to 9 years old and 10 to 16 years old) and compared mean FD values between males and females in each age group. Age characteristics and the number of participants of each age group were taken into account when determining the groups (Table 3). We observed significant sex differences across F1 to F4 in the age group of 7 to 9 years ($p < 0.05$, two tails, dof = 27, FDR corrected) with boys moving more than girls (Fig. 8b) while the difference was not significant for F5. The raw t-values and p-values of these comparisons are: F1, t = -2.300, p = 0.029, r2 = 0.164, Cohen's d = 0.098; F2, t = -2.240, p = 0.033, r2 = 0.157, Cohen's d = 0.069; F3, t = -2.324, p = 0.027, r2 = 0.167, Cohen's d =0.059; F4, t = -2.323, p = 0.028, r2 = 0.167, Cohen's d = 0.050; F5, t = -1.939, p = 0.063, r2 = 0.122, Cohen's d = 0.032. No such sex-related effects on head motion were detectable for the other age groups. As Fig. 7b also shows, boys were substantially more variable than girls across all five frequency intervals. The variation values of both boys and girls in this age range are shown in Table 4.

Table 3 Age groups

Age group	Number of males	Number of females	Total number
3 to 6 years old	14	18	32
7 to 9 years old	14	15	29
10 to 16 years old	14	9	23

Table 4 Descriptive statistics of mean FD values of children between 7 to 9 years old

Sex	Frequency	Mean	Standard deviation	Number
Female	F1	0.0260941667	0.02298396159	15
	F2	0.0309419333	0.02252424263	15
	F3	0.0328717333	0.01212196762	15
	F4	0.0394202000	0.00943084342	15
	F5	0.0573435333	0.01262457056	15
Male	F1	0.0723681643	0.07429027709	14
	F2	0.0782372857	0.07845646646	14
	F3	0.0673085000	0.05560847182	14
	F4	0.0675354286	0.04590004007	14
	F5	0.0758437857	0.03460116143	14

5 DREAM Demo2: Spatial ranks of ALFF across frequencies

The amplitude of low frequency fluctuation (ALFF) is a common measure used in fMRI studies that reflects regional amplitude of the signal intensity's fluctuations in a frequency range (Zang et al., 2007). Previous studies revealed variations of ALFF in both spatial and frequency domains in the resting-state brain. From the perspective of spatial distribution, in the typical resting-state frequency range (e.g., 0.01-0.1 Hz), the neural oscillations showed higher ALFF in grey matter than white matter (Turner et al., 1993; Biswal et al., 1995). ALFF reaches its peaks in visual areas (Kiviniemi et al., 2003), posterior structures along brain midline (Zang et al., 2007; Zou et al., 2009) and in cingulate and medial prefrontal cortices (Ghosh rt sl., 2008). In frequency domain, BOLD oscillations distributed to grey matter were mainly in slow-4 and slow-5, while its white matter oscillations were dominated by slow-3 and slow-2 (Zuo et al., 2010). Specifically, higher ALFF in slow-4 was detected in the bilateral thalamus and basal ganglia whereas the slow-5 oscillators exhibited higher ALFF in the ventromedial prefrontal cortex, precuneus and cuneus (see a replication study from Xue et al., 2014). These findings revealed the frequency-specific characteristics of resting-state ALFF. Limited by the sampling precision (T_R = 2000ms), studies on the ALFF distribution across more accurate bands and their reliabilities are still lacking. For examples, the slow-2 frequency band derived in Zuo et al. (2010) has quite small overlap with its theoretical range and thus may limit both reliability and validity of its findings. Here, we use DREAM to decompose the fast (T_R = 720ms) rfMRI data from the Human Connectome Project (HCP) (Van Essen et al., 2013) test-retest dataset, to 1) map the ranks of ALFF values through slow-1, slow-2, show-3, slow-4 and slow-5 bands and 2) evaluate the test-retest reliability of the ALFF values in these different frequency bands.

5.1 Participants and data acquisition

The test-retest dataset from HCP consisting of 45 subjects were used for this analysis. All subjects were scanned with an HCP-customized Siemens 3T scanner at Washington University, using a standard 32-channel receive head coil. Three participants were excluded from the substantial analyses because their resting-state scan durations were shorter than others. Forty-two subjects (aged 30.3 ± 3.4 years, 29 males) were included in the present study. Each subject was scanned two times and each scan contained structural images (T1w and T2w), two rfMRI, seven runs of task fMRI and high angular

resolution diffusion imaging (see details of the imaging protocols from HCP website[4]). Of note, in the present work, we only used the rfMRI data, which consisted of 1200 volumes (T_R = 720 ms; TE = 33.1 ms; flip angle = 52°, 72 slices, matrix = 104×90; FOV = 208x180 mm; acquisition voxel size = 2×2×2 mm). The data were preprocessed according to the HCP MR preprocessing pipeline (Glasser et al., 2013), resulting in the preprocessed surface time series data fed to the following DREAM analysis.

5.2 ALFF analysis

For each rfMRI scan, we first extracted the representative time series for each of the 400 parcels (Schaefer et al., 2018) by averaging all the preprocessed time series within a single parcel. DREAM decomposed the time series into its components across the potential frequency bands. We performed ALFF analysis for all the bands of each run and each subject according to (Zuo et al., 2010) implemented by CCS (Xu et al., 2015). Subject-level parcel-wise ALFF maps for each frequency band were standardized into subject-level Z-score maps (i.e., by subtracting the mean parcel-wise ALFF of the entire cortical surface, and dividing by the standard deviation). The two standardized ALFF maps in the same session were then averaged, resulting in two (test versus retest) standardized ALFF maps per frequency band for each subject. To investigate the test-retest reliability of ALFF across the five frequency bands, we calculated the parcel-wise intraclass correlation (ICC) based upon the two ALFF maps (Zuo et al., 2013; Xing & Zuo, 2018). We averaged the two standardized ALFF maps of all the subjects to obtain the group-level standardized ALFF maps. In order to evaluate the spatial distribution of the ALFF values for each parcel, we assigned its rank of ALFF values to the parcel (from 1 to 400). All the above analyses were done for each of the five frequency bands, leading to an ALFF ranking map for each frequency band.

5.3 Results

DREAM decomposed the rfMRI timeseries into five frequency bands (slow-5: 0.012-0.030 Hz; slow-4: 0.030-0.082 Hz; slow-3: 0.082-0.223 Hz; slow-2: 0.223-0.607 Hz; slow-1: 0.607-0.694 Hz). Figure 9 mapped ALFF regarding its ranking and reliability for all the frequency bands. It is clear that ALFF ranked from high in ventral-temporal areas to low in ventral-occipital areas when the frequency band increased from low to high, while those in part of parietal and ventral frontal regions were reversed. In terms of the ICC maps, it is generally true that the higher frequency bands, the more reliable ALFF measurements. The slow-2 (0.223-0.607 Hz) demonstrated the highest test-retest reliability of ALFF across the five frequency bands.

6 Discussion

DREAM is free and publicly available software that can decode oscillation data into multiple frequency bands. The simple interface was designed to allow all users to easily perform multi-band frequency analyses. The computational methods employed in DREAM to calculate the numbers and ranges of decoded frequency bands apply the Nyquist-Shannon sampling theorem. This toolbox is applicable for multiple forms of discrete sampling data, as long as the data are entered in the supported format. Currently,

[4] http://protocols.humanconnectome.org/HCP/3T/imaging-protocols.html

DREAM can process both NIFTI formatted neuro imaging data and text file formatted behavioral data. Additional supported formats will be forthcoming.

As a demonstration of its utility, the results derived with DREAM for pure behavioral recordings suggest that head motion may be a behavioral feature reflecting both state and trait of individuals. As hypothesized, young children moved more than older children. This observation was more evident in the higher frequency bands than in the lower frequency bands, which reflects more sudden and sharp movements in younger children. The stability of head motion during the experiment also varied with age, with head motion becoming less variable in older children. A specific age range (7 - 9 years) was associated with sex effects on head motion, with boys tending to move more than girls across F1 to F4 bands. The sex-related differences in head motion was greater in lower frequency intervals than in higher frequency intervals. This might be an indication that this age range is a key period for developing the ability to apply effective cognitive control. Our findings are consistent with recent reports that head motion during fMRI scanning can be an important confounding factor (Power et al., 2015) while it also has neurobiological components related to individual motion traits (Zeng et al., 2014; Zhou et al., 2016), which are likely driven by brain systems operating within a multi-band frequency landscape. Our results demonstrate the necessity to study the characteristics of head motion especially in special cohorts like children, the elderly and patients with neurologic or psychiatric conditions, since differences of distance-related functional connectivity that may be influenced by head motion have been observed between such special cohorts and healthy young adults (Andrews-Hanna et al., 2007; Fair et al., 2007; Satterthwaite et al., 2012; Fair et al., 2013).

Differences in head motion across ages or between cohorts may reflect differences of certain traits, which may co-vary with detected brain signals and behavioral observations. The different properties of head motion in different frequency bands show that there may be different mechanisms associated with different frequencies. Head motion at higher frequencies varies more with age, and this may reflect that cognitive control associated with higher frequencies develops better with age. Of note, interpolation analyses indicated that this observation is not related to an issue of better signal-to-noise ratio at higher frequencies because there are more events per unit time. Within the narrow age range of 7 to 9 years old, boys moved more than girls in most frequency bands, although sex differences were larger at lower frequencies. This may indicate that the development of controlling system associated with lower frequencies may have larger sex-related differences for this age range. The above results lead us to speculate that there may be two control systems that are associated with different frequency bands of head motion which develop differently with age and between boys and girls. More detailed experimental studies are needed to test this postulation in future. The strategies of dealing with head motion issue in human brain mapping may also need updates regarding its measurement reliability and validity in terms of the possible neurobiological correlates (Xing & Zuo., 2018; Zuo et al., 2019a; Zuo et al., 2019b).

We detected the pattern of ALFF ranking gradually from low to high frequency bands, indicating a trend along the two orthogonal axes. Along the dorsal-ventral axis, higher ALFF ranks were moving from the ventral occipital and the ventral temporal lobe up to regions in the parietal lobe as the frequency increasing. Along the anterior-posterior axis, from lower to higher bands, higher ALFF ranks were walking from the posterior to the anterior regions in the ventral part. Such a frequency-dependent ALFF pattern is

similar to the findings of previous studies on the association between brain structure and gene expression, which also reported orthogonal gradations of brain organization and the associated genetic gradients (Chen et al., 2013; Kremen et al., 2013). The underlying physiological mechanism and functional significance of the frequency-dependent ALFF patterns deserve further investigations. It is interesting that the frequency-dependent pattern of ICC is quite uniform across the brain and as the frequency increased, its reliability increased alongside. This observation illustrated that compared with the low frequency bands, higher frequency bands might be more suitable for detecting individual differences in ALFF. Most of the previous studies have adopted ALFF of the lower frequency bands (i.e., slow-5 and slow-4 or around 0.01 to 0.1 Hz) where their ICCs rarely met the reliability requirement (>= 0.8) of clinical applications. In contrast, our findings suggest that both slow-2 and slow-1 ALFF could be the usable and reliable marker of the brain oscillations for these applications. It is noticed that the reliability of slow-1 ALFF is slightly lower than those of slow-2 ALFF, and this may be an indication on the limited slow-1 band here compared to its theoretical range, i.e., around 0.6065-1.6487 Hz. While studies of the very fast sampled fMRI signals such as HCP are sparse, it is quite promising for future studies with multiple neuroimaging modalities (e.g., Balduzzi et al., 2008; He et al., 2008) including fMRI[5], EEG[6], MEG and ECoG using DREAM as an integrative tool across frequencies. An open toolbox such as DREAM is essential for large-scale projects inspired by the increasing practice of open sciences coming with more and more fMRI and EEG datasets openly shared.

7 Information sharing statement

The DREAM toolbox (https://github.com/zuoxinian/CCS/tree/master/H3/DREAM) has been made open to the public. More details of its usage are documented as the online resource. Please credit or cite both DREAM and CCS paper if you use DREAM.

8 Funding

This work was supported in part by the China - Netherlands CAS-NWO Programme (153111KYSB20160020), Beijing Municipal Science and Technology Commission (Z161100002616023, Z171100000117012), the National R&D Infrastructure and Facility Development Program of China, Fundamental Science Data Sharing Platform (DKA2019-12-02-21), and Guangxi BaGui Scholarship (201621). The neuroimaging data were provided by the HCP WU-Minn Consortium, which is funded by the 16 NIH institutes and centers that support the NIH Blueprint for Neuroscience Research 1U54MH091657 (PIs: David Van Essen and Kamil Ugurbil), the McDonnell Center for Systems Neuroscience at Washington University.

9 Conflict of Interest Statement

The authors declare that the research was conducted in the absence of any commercial or financial relationships that could be construed as a potential conflict of interest.

[5] https://climbgroup.org/databases/
[6] https://github.com/meagmohit/EEG-Datasets

References

Andrewshanna, J. R., Snyder, A. Z., Vincent, J. L., Lustig, C., Head, D., Raichle, M. E., & Buckner, R. L. (2007). Disruption of large-scale brain systems in advanced aging. Neuron, 56(5), 924.

Biswal, B., Yetkin, F. Z., Haughton, V. M., & Hyde, J. S. (1995). Functional connectivity in the motor cortex of resting human brain using echo-planar MRI. Magnetic Resonance in Medicine, 34(4), 537-541.

Buzsaki, G., & Draguhn, A. (2004). Neuronal oscillations in cortical networks. Science, 304(5679), 1926-1929.

Balduzzi, D., Riedner, B. A. & Tononi, G. (2008). A BOLD window into brain waves. Proceedings of the National Academy of Sciences of the United States of America, 105(41), 15641-15642.

Chen, C. H., Fiecas, M., Gutierrez, E. D., Panizzon, M. S., Eyler, L. T., Vuoksimaa, E., Thompson, W. K., Fennema-Notestine, C., Hagler, D. J., Jernigan, T. L., Neale, M. C., Franz, C. E., Lyons, M. J., Fischl, B., Tsuang, M. T., Dale, A. M., & Kremen, W. S. (2013). Genetic topography of brain morphology. Proceedings of the National Academy of Sciences of the United States of America, 110(42), 17089-17094.

Di Martino, A., Ghaffari, M., Curchack, J., Reiss, P., Hyde, C., Vannucci, M., Petkova, E., Klein, D. F., & Castellanos, F. X. (2008). Decomposing intra-subject variability in children with attention-deficit/hyperactivity disorder. Biological Psychiatry, 64(7), 607-614.

Fair, D. A., Dosenbach, N. U., Church, J. A., Cohen, A. L., Brahmbhatt, S., Miezin, F. M., Barch, D. M., Raichle, M. E., Petersen, S. E., & Schlaggar, B. L. (2007). Development of distinct control networks through segregation and integration. Proceedings of the National Academy of Sciences of the United States of America, 104(33), 13507-13512.

Fair, D. A., Nigg, J. T., Iyer, S., Bathula, D., Mills, K. L., Dosenbach, N. U., Schlaggar, B. L., Mennes, M., Gutman, D., & Bangaru, S. (2013). Distinct neural signatures detected for ADHD subtypes after controlling for micro-movements in resting state functional connectivity MRI data. Frontiers in Systems Neuroscience, 6(80), 80.

Ghosh, A., Rho, Y., McIntosh, A. R., Kotter, R., & Jirsa, V. K. (2008). Noise during rest enables the exploration of the brain's dynamic repertoire. Plos Computational Biology, 4(10), 12.

Glasser, M. F., Sotiropoulos, S. N., Wilson, J. A., Coalson, T. S., Fischl, B., Andersson, J. L., Xu, J., Jbabdi, S., Webster, M., Polimeni, J. R., Van Essen, D. C., Jenkinson, M., & Consortium, W. U.-M. H. (2013). The minimal preprocessing pipelines for the Human Connectome Project. Neuroimage, 80, 105-124.

Han, Y., Wang, J., Zhao, Z., Min, B., Lu, J., Li, K., He, Y., & Jia, J. (2011). Frequency-dependent changes in the amplitude of low-frequency fluctuations in amnestic mild cognitive impairment: A resting-state fMRI study. Neuroimage, 55(1), 287-295.

He, B. J., Snyder, A. Z., Zempel, J. M., Smyth, M. D., Raichle, M. E. (2008). Electrophysiological correlates of the brain's intrinsic large-scale functional architecture. Proceedings of the National Academy of Sciences of the United States of America, 105(41), 16039-16044.

Jing, L.-L., Huang, L.-Y., Huang, D.-F., Niu, J., & Zhong, Z. (2012). Amplitude of low frequency fluctuation at different frequency bands in early amnestic mild cognitive impairment: results from ADNI. Journal of Innovative Optical Health Sciences, 5(1).

Kiviniemi, V., Kantola, J. H., Jauhiainen, J., Hyvarinen, A., & Tervonen, O. (2003). Independent component analysis of nondeterministic fMRI signal sources. Neuroimage, 19(2), 253-260.

Kremen, W. S., Fennema-Notestine, C., Eyler, L. T., Panizzon, M. S., Chen, C.-H., Franz, C. E., Lyons, M. J., Thompson, W. K., & Dale, A. M. (2013). Genetics of brain structure: Contributions from the vietnam era twin study of aging. American Journal of Medical Genetics Part B-Neuropsychiatric Genetics, 162(7), 751-761.

Li, Y., Jing, B., Liu, H., Li, Y., Gao, X., Li, Y., Mu, B., Yu, H., Cheng, J., Barker, P. B., Wang, H., & Han, Y. (2017). Frequency-dependent changes in the amplitude of low-frequency fluctuations in mild cognitive impairment with mild depression. Journal of Alzheimers Disease, 58(4), 1175-1187.

Lowe, M. J., Mock, B. J., & Sorenson, J. A. (1998). Functional connectivity in single and multislice echoplanar imaging using resting-state fluctuations. Neuroimage, 7(2), 119-132.

Mascali, D., DiNuzzo, M., Gili, T., Moraschi, M., Fratini, M., Maraviglia, B., Serra, L., Bozzali, M., & Giove, F. (2015). Intrinsic patterns of coupling between correlation and amplitude of low-frequency fMRI fluctuations are disrupted in degenerative dementia mainly due to functional disconnection. Plos One, 10(4).

Penttonen, M., & Buzsáki, G. (2003). Natural logarithmic relationship between brain oscillators. Thalamus & Related Systems, 2(2), 145-152.

Power, J. D., Barnes, K. A., Snyder, A. Z., Schlaggar, B. L., & Petersen, S. E. (2012). Spurious but systematic correlations in functional connectivity MRI networks arise from subject motion. Neuroimage, 59(3), 2142-2154.

Power, J. D., Schlaggar, B. L., & Petersen, S. E. (2015). Recent progress and outstanding issues in motion correction in resting state fMRI. Neuroimage, 105, 536-551.

Ren, P., Lo, R. Y., Chapman, B. P., Mapstone, M., Porsteinsson, A., Lin, F., & Alzheimer's Dis Neuroimaging, I. (2016). Longitudinal alteration of intrinsic brain activity in the striatum in mild cognitive impairment. Journal of Alzheimers Disease, 54(1), 69-78.

Satterthwaite, T. D., Wolf, D. H., Loughead, J., Ruparel, K., Elliott, M. A., Hakonarson, H., Gur, R. C., & Gur, R. E. (2012). Impact of in-scanner head motion on multiple measures of functional connectivity: Relevance for studies of neurodevelopment in youth. Neuroimage, 60(1), 623-632.

Schaefer, A., Kong, R., Gordon, E. M., Laumann, T. O., Zuo, X.-N., Holmes, A. J., Eickhoff, S. B., & Yeo, B. T. T. (2018). Local-Global Parcellation of the Human cerebral cortex from intrinsic functional connectivity MRI. Cerebral Cortex, 28(9), 3095-3114.

Turner, R., Jezzard, P., Wen, H., Kwong, K. K., Lebihan, D., Zeffiro, T., & Balaban, R. S. (1993). Functional mapping of the human visual-cortex at 4 and 1.5 tesla using deoxygenation contrast EPI. Magnetic Resonance in Medicine, 29(2), 277-279.

Van Essen, D. C., Smith, S. M., Barch, D. M., Behrens, T. E. J., Yacoub, E., Ugurbil, K., & Consortium, W. U.-M. H. (2013). The WU-Minn Human Connectome Project: An overview. Neuroimage, 80, 62-79.

Wang, P., Li, R., Yu, J., Huang, Z., & Li, J. (2016). Frequency-dependent brain regional homogeneity alterations in patients with mild cognitive impairment during working memory state relative to resting state. Frontiers in Aging Neuroscience, 8.

Xing, X.-X., & Zuo, X.-N. (2018). The anatomy of reliability: a must read for future human brain mapping. Science Bulletin, 63(24), 1606-1607.

Xu, T., Yang, Z., Jiang, L., Xing, X.-X., & Zuo, X.-N. (2015). A Connectome Computation System for discovery science of brain. Science Bulletin, 60(1), 86-95.

Xue, S. W., Li, D., Weng, X. C., Northoff, G., & Li, D. W. (2014). Different neural manifestations of two slow frequency bands in resting functional magnetic resonance imaging: a systemic survey at regional, interregional, and network levels. Brain Connect, 4(4), 242-255.

Yan, C.-G., Craddock, R. C., He, Y., & Milham, M. P. (2013). Addressing head motion dependencies for small-world topologies in functional connectomics. Frontiers in Human Neuroscience, 7.

Yang, N., He, Y., Zhang, Z., Dong, H., Zhang, L., Zhu, X., Hou, X., Wang, Y., Zhou, Q., Gong, Z., Cao, L., Wang, P., Zhang, Y., Sui, D., Xu, T., Wei, G., Yang, Z., Jiang, L., Li, H., Feng, T., Chen, A., Qiu, J., Chen, X., & Zuo, X. (2017). Chinese Color Nest Project: Growing up in China. [彩巢计划成长在中国]. Chinese Science Bulletin, 62(26), 3008-3022.

Zang, Y. F., He, Y., Zhu, C. Z., Cao, Q. J., Sui, M. Q., Liang, M., Tian, L. X., Jiang, T. Z., & Wang, Y. F. (2007). Altered baseline brain activity in children with ADHD revealed by resting-state functional MRI. Brain & Development, 29(2), 83-91.

Zeng, L. L., Wang, D. H., Fox, M. D., Sabuncu, M., Hu, D. W., Ge, M., Buckner, R. L., & Liu, H. S. (2014). Neurobiological basis of head motion in brain imaging. Proceedings of the National Academy of Sciences of the United States of America, 111(16), 6058-6062.

Zhao, Z.-L., Fan, F.-M., Lu, J., Li, H.-J., Jia, L.-F., Han, Y., & Li, K.-C. (2015). Changes of gray matter volume and amplitude of low-frequency oscillations in amnestic MCI: An integrative multi-modal MRI study. Acta Radiologica, 56(5), 614-621.

Zhou, Y., Chen, J., Luo, Y., Zheng, D., Rao, L.-L., Li, X., Zhang, J., Li, S., Friston, K., & Zuo, X.-N. (2016). Genetic overlap between in-scanner head motion and the default network connectivity. bioRxiv.

Zou, Q. H., Wu, C. W., Stein, E. A., Zang, Y. F., & Yang, Y. H. (2009). Static and dynamic characteristics of cerebral blood flow during the resting state. Neuroimage, 48(3), 515-524.

Zuo, X. N., Di Martino, A., Kelly, C., Shehzad, Z. E., Gee, D. G., Klein, D. F., Castellanos, F. X., Biswal, B. B., & Milham, M. P. (2010). The oscillating brain: Complex and reliable. Neuroimage, 49(2), 1432-1445.

Zuo, X. N., Xu, T., Jiang, L., Yang, Z., Cao, X. Y., He, Y., Zang, Y. F., Castellanos, F. X., Milham, M. P. (2013). Toward reliable characterization of functional homogeneity in the human brain: preprocessing, scan duration, imaging resolution and computational space. Neuroimage, 65, 374-386.

Zuo, X.-N., Biswal, B. B., & Poldrack, R. A. (2019). Editorial: Reliability and reproducibility in functional connectomics. Frontiers in Neuroscience, 13.

Zuo, X.-N., He, Y., Betzel, R. F., Colcombe, S., Sporns, O., & Milham, M. P. (2017). Human connectomics across the life span. Trends in Cognitive Sciences, 21(1), 32-45.

Zuo, X.-N., Xu, T., & Milham, M. P. (2019). Harnessing reliability for neuroscience research. Nature Human Behaviour, 3(8), 768-771.

Figures

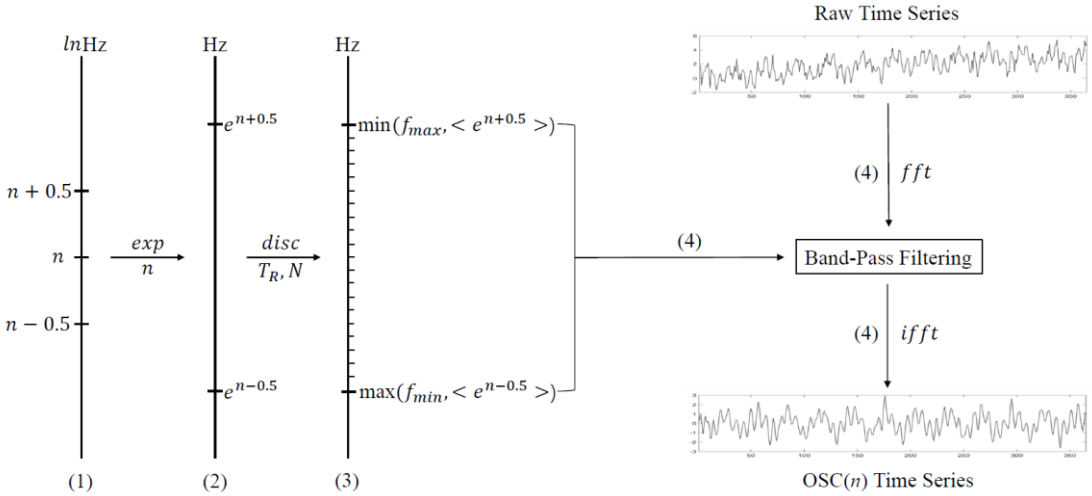

Fig. 1 The flowchart on the DREAM algorithm. (1) N3L theory defines an oscillator with a length-one frequency band centered at n, i.e., OSC(n), in the natural log space. (2) In original frequency space, it expands the frequency band $\boldsymbol{e}^{n+0.5}$-$\boldsymbol{e}^{n-0.5}$ Hz. (3) This frequency band can be discretized with a sampling procedure with N points and T_R rate in terms of the classical signal theory. (4) This computational frequency band is for a band-pass filtering process to extract the OSC(n) from the raw time series.

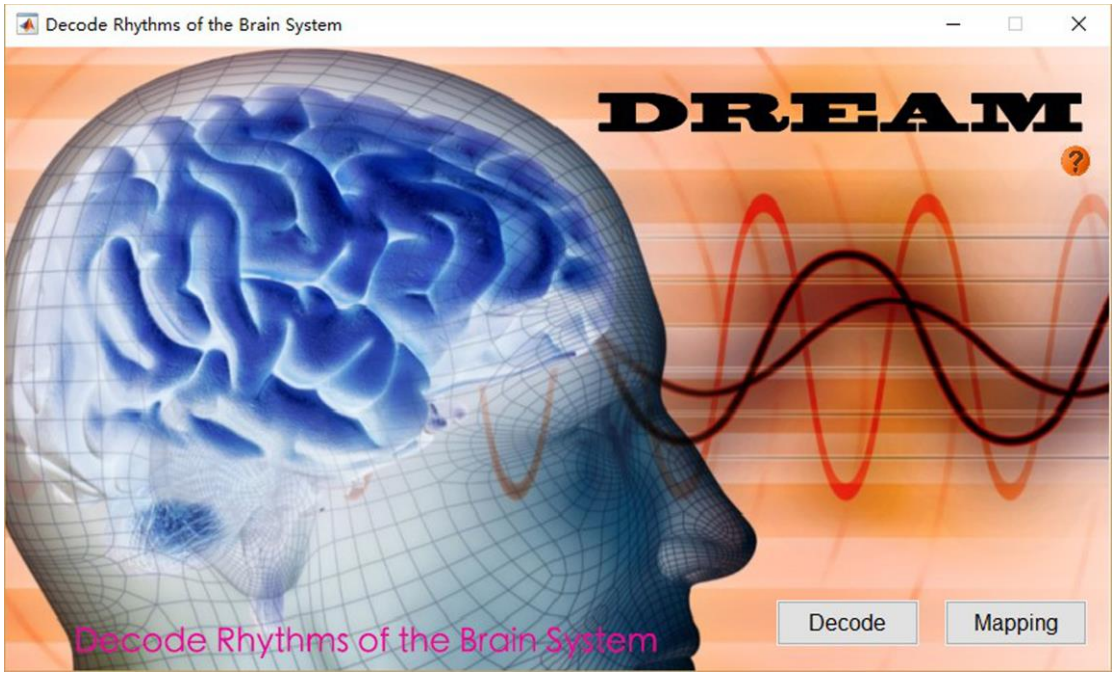

Fig. 2 The DREAM welcome screen

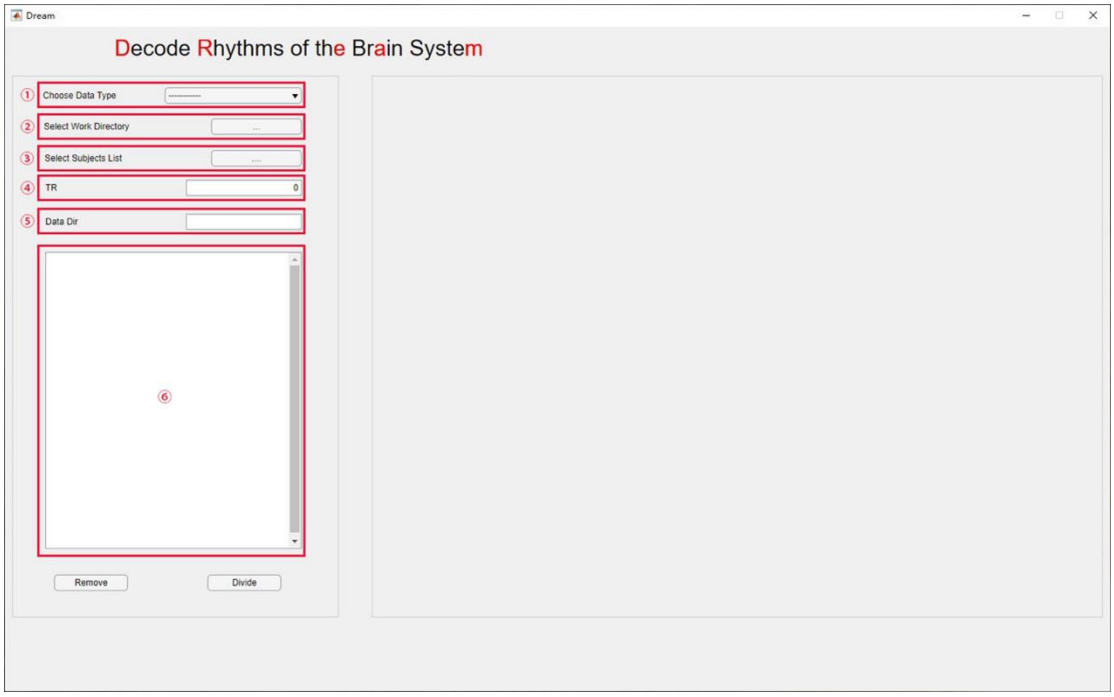

Fig. 3 The main interface of DREAM. Circled numbers correspond to the usage steps introduced in the *3.2 GUI Usage* section

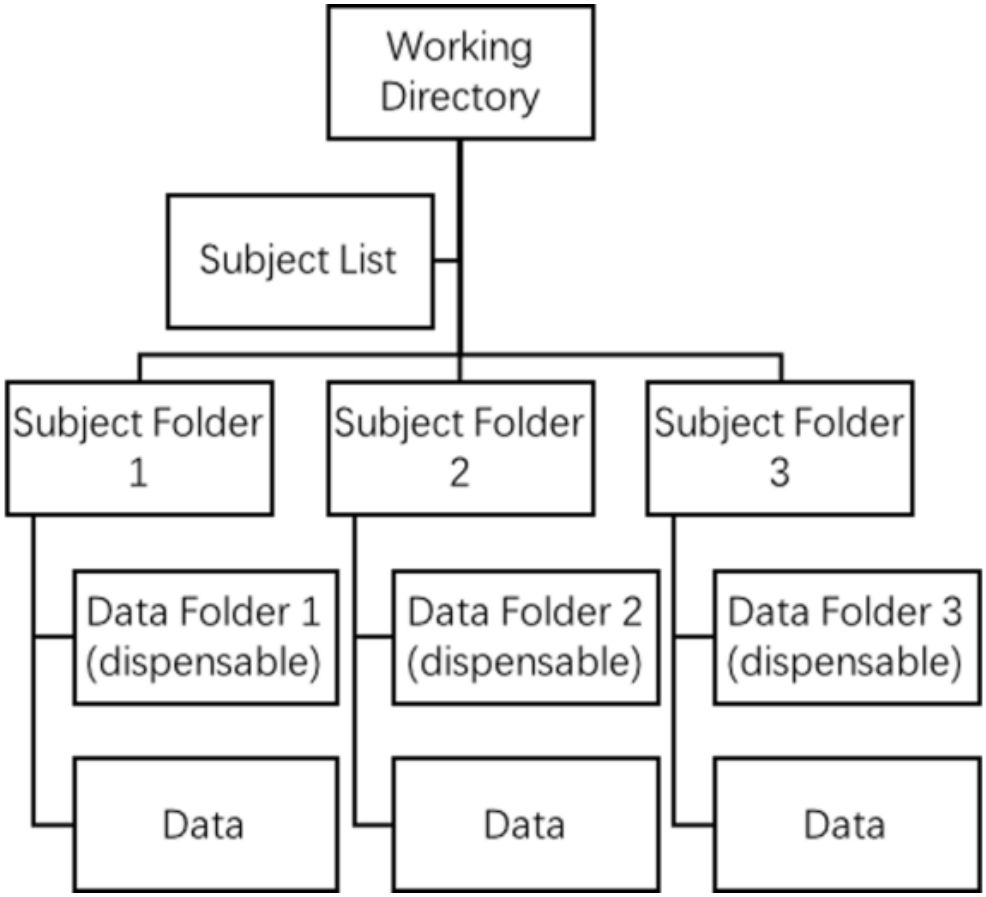

Fig. 4 Data structure for processing by DREAM

Fig. 5 The mock MRI scanner at CLIMB

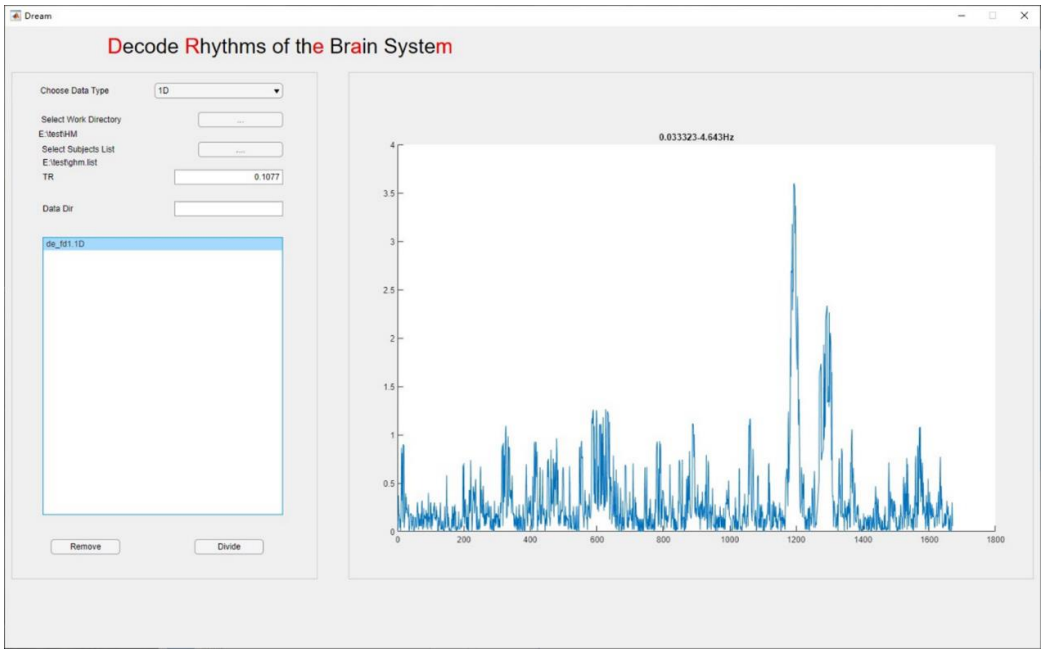

Fig. 6 A preview of the original FD time series from a participant

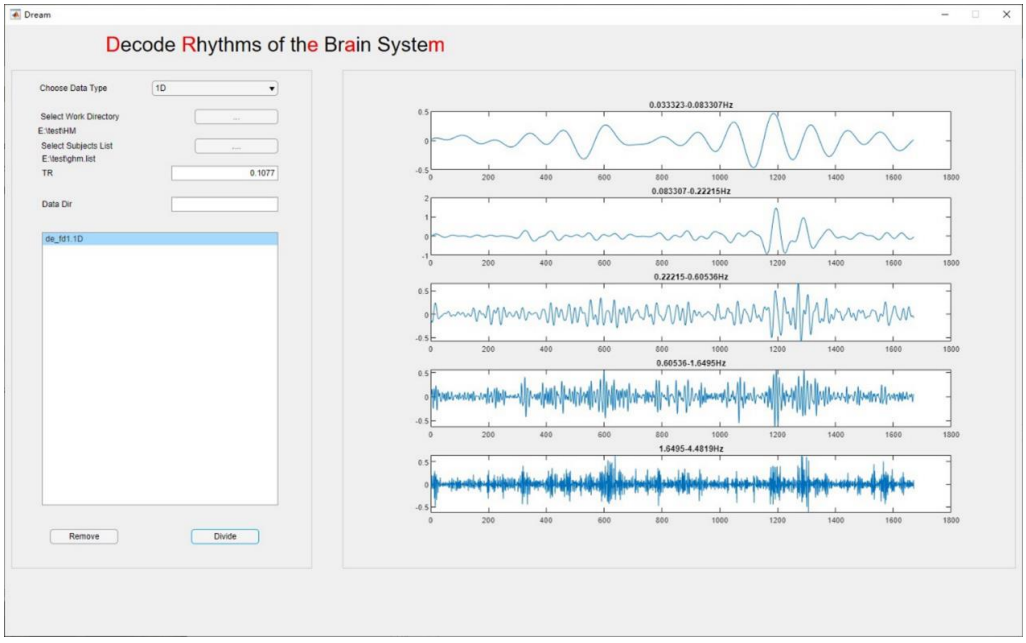

Fig. 7 DREAM decodes FD time series from the participant into five bands.

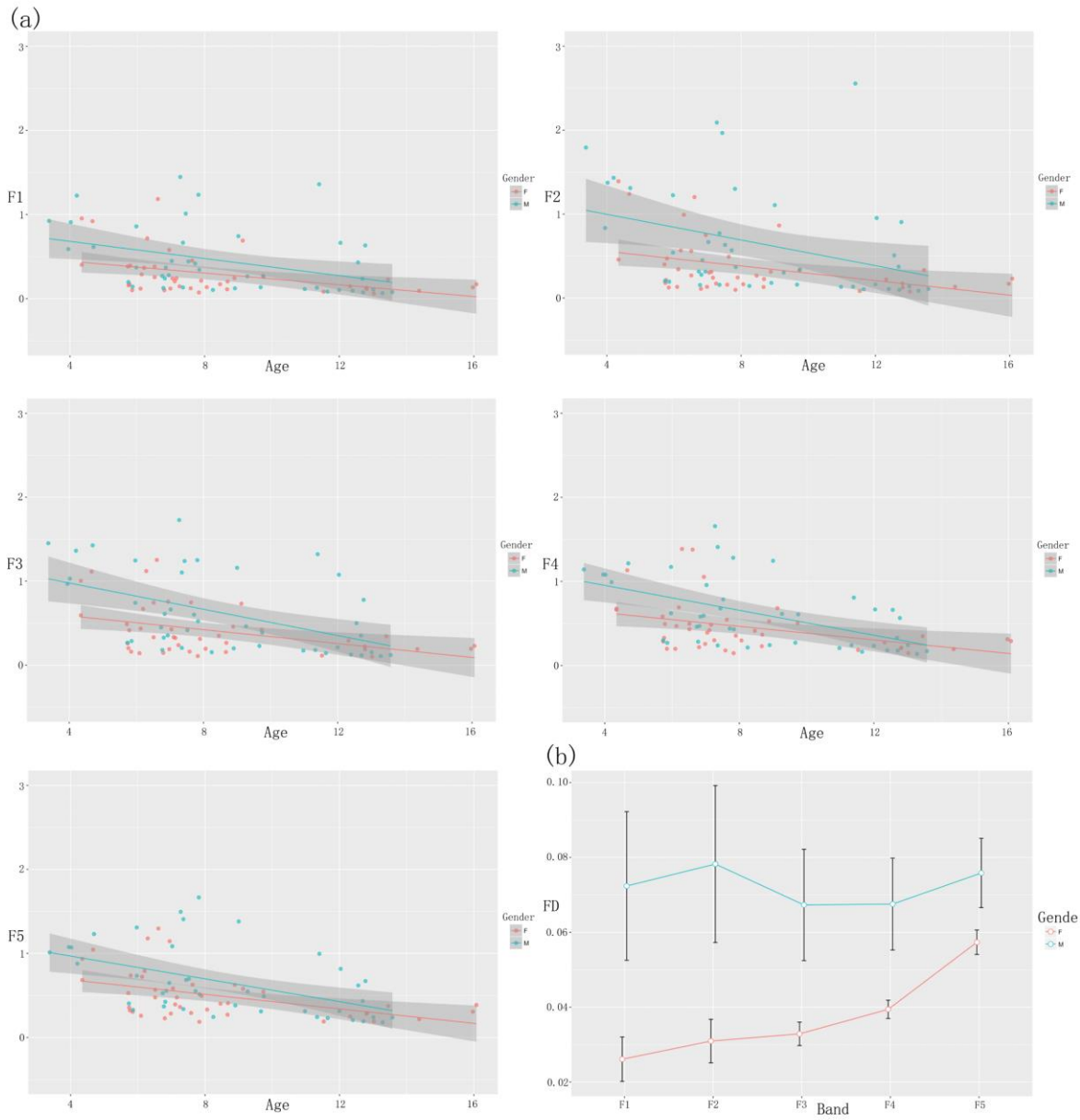

Fig. 8 (a) Negative correlations between age and mean FD values of all five frequency bands. (b) Boys moved more than girls across F1 to F4 bands in the age range of 7-9 years.

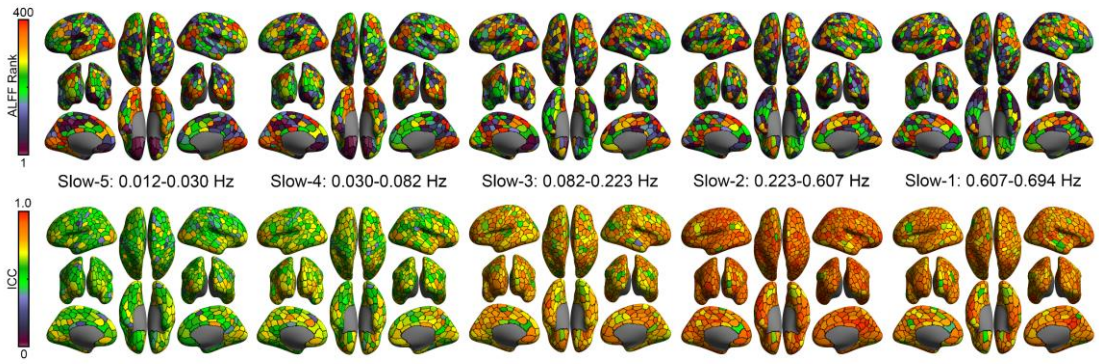

Fig 9. Mapping ALFF and its reliability across slow frequency bands.